Chapter 6
Holonomic rolling nonprehensile manipulation primitive

Alejandro Donaire, Fabio Ruggiero, Vincenzo Lippiello, Bruno Siciliano

Abstract In this chapter, the design of nonlinear controllers for non-prehensile holonomic rolling system is reviewed. A general model for the class of non-prehensile rolling system considered in this work is first formulated. Then, both the input-state linearisation approach and the interconnection and damping assignment passivity-based control technique for rolling systems are addressed. The class of control designs presented in this chapter make use of energy concepts and physical properties. Three benchmark examples are used to illustrate the control design presented, namely the disk-on-disk, the ball-and-beam, and the eccentric disk-on-disk
This chapter is based on the works presented in [82, 173, 277].

Alejandro Donaire
The University of Newcastle, University Drive, Callaghan, 2308, NSW, Australia, e-mail: alejandro.donaire@newcastle.edu.eu

Fabio Ruggiero
CREATE Consortium & University of Naples Federico II, Department of Electrical Engineering and Information Technology, PRISMA Lab, Via Claudio 21, 80125, Naples, Italy, e-mail: fabio.ruggiero@unina.it

Vincenzo Lippiello
CREATE Consortium & University of Naples Federico II, Department of Electrical Engineering and Information Technology, PRISMA Lab, Via Claudio 21, 80125, Naples, Italy, e-mail: vincenzo.lippiello@unina.it

Bruno Siciliano
CREATE Consortium & University of Naples Federico II, Department of Electrical Engineering and Information Technology, PRISMA Lab, Via Claudio 21, 80125, Naples, Italy, e-mail: bruno.siciliano@unina.it

Table 6.1: Main symbols used in this chapter.

Definition	**Symbol**
Frame attached to the CoM of the hand	$\mathcal{H}$
Frame attached to the CoM of the object	$\mathcal{O}$
Angle of the hand in $\mathcal{W}$	$\theta_h \in \mathbb{R}$
Position of $\mathcal{H}$ in $\mathcal{W}$	$\mathbf{p}_h(\theta_h) \in \mathbb{R}^2$
Position of $\mathcal{O}$ in $\mathcal{W}$	$\mathbf{p}_o \in \mathbb{R}^2$
Angle of the object in $\mathcal{W}$	$\theta_o \in \mathbb{R}$
Arclength parameter for the hand	$s_h \in \mathbb{R}$
Arclength parameter for the object	$s_o \in \mathbb{R}$
Rotation of $\mathcal{H}$ with respect to $\mathcal{W}$	$\mathbf{R}(\theta_h) \in SO(2)$
Rotation of $\mathcal{O}$ with respect to $\mathcal{W}$	$\mathbf{R}(\theta_o) \in SO(2)$
Configuration vector	$\mathbf{q} = \begin{bmatrix} q_1 & q_2 \end{bmatrix}^T \in \mathbb{R}^2$
Mass matrix	$\mathbf{M}(q) = \begin{bmatrix} m_{11}(\mathbf{q}) & m_{12}(\mathbf{q}) \\ m_{12}(\mathbf{q}) & m_{22}(\mathbf{q}) \end{bmatrix} \in \mathbb{R}^{2\times 2}$
Coriolis matrix	$\mathbf{C}(q,\dot{q}) = \begin{bmatrix} c_{11} & c_{12} \\ c_{21} & c_{22} \end{bmatrix} \in \mathbb{R}^{2\times 2}$
Gravity vector	$\mathbf{g}(\mathbf{q}) = \begin{bmatrix} g_1(\mathbf{q}) & g_2(\mathbf{q}) \end{bmatrix}^T \in \mathbb{R}^2$
Inertia of the hand	$I_h \in \mathbb{R}$
Mass of the hand	$m_h > 0$
Inertia of the object	$I_o \in \mathbb{R}$
Mass of the object	$m_o > 0$
Gravity acceleration	$g = 9.81$ m/s^2
Selection vector	$\mathbf{e}_= \begin{bmatrix} 0 & 1 \end{bmatrix}^T \in \mathbb{R}^2$
Momentum vector	$\mathbf{p} = \mathbf{M}(\mathbf{q})\dot{\mathbf{q}} \in \mathbb{R}^n$
Hand torque applied at the hand's center of rotation	$\tau_h \in \mathbb{R}$
Hand acceleration	$a_h \in \mathbb{R}$
Radius of the actuated disk (DoD and eccentric DoD setups)	$\rho_h > 0$
Radius of the upper disk (DoD setup and eccentric DoD setups) and radius of the rolling ball (BnB setup)	$\rho > 0$
Distance between the beam's CoM and its surface where the ball rolls (BnB setup)	$d_h > 0$
Hamiltonian function	$H : \mathbb{R}^4 \to \mathbb{R}$
Desired Hamiltonian function	$H_d : \mathbb{R}^4 \to \mathbb{R}$
Desired mass matrix	$\mathbf{M}_d(q) \in \mathbb{R}^{2\times 2}$

6.1 Brief introduction

The manipulation problem of nonprehensile planar rolling concerns tasks that involve an actuated manipulator, which in this chapter is called the hand, and an object that is manipulated without form or force closure grasps [252]. There exist many examples of such robotic systems, the *disk-on-disk* [83, 265], the *ball-and-beam* [126, 236], and the *butterfly robot* [49, 184, 303] among the benchmarks presented in the literature. In detail, DoD is composed of an up-

per disk (object) that can roll without slipping on the rim of a lower actuated disk (hand). The BnB consists of a beam (hand) actuated by a torque around its CoM together with a ball (object) rolling on it. The butterfly robot is composed of an actuated butterfly-shaped link (hand) and a ball (object) that can freely roll on the rim of the link. The control objective in these examples is to balance the object and drive the hand towards the desired configuration. The shared characteristic of these planar systems is the holonomic nature of the pure rolling constraint. A constraint is said to be holonomic if it comes from an integrable kinematic constraint that can be expressed in the so-called Pfaffian form [284]. The integrability condition allows instantaneous motion in every admissible direction, that is just one in the case of planar systems like the ones addressed in this chapter.

This chapter presents control designs for nonprehensile planar rolling systems based on two techniques: input-state FLin and IDA-PBC. The designs are illustrated on two benchmarks, namely the disk-on-disk and the ball-and-beam systems. In addition, a different system, referred to as eccentric DoD, is used to demonstrate a novel procedure to design IDA-PBC controllers. This last example is a variant of the DoD system, where the center of rotation of the hand and its geometric center are not coincident.

This chapter is organised as follows. First, a general model of nonprehensile planar rolling systems is presented. Then, a control design based on FLin is presented to design controllers for nonprehensile planar rolling systems. In a subsequence section, the IDA-PBC technique is used to design controllers for nonprehensile planar rolling systems. In each section, the control designs are applied to all or some of the benchmark examples. The chapter is wrapped up with discussion and conclusions.

6.2 Dynamic model of nonprehensile holonomic rolling manipulation systems

In this section, the model of a general class of nonprehensile planar rolling systems shown in Fig. 6.1 is formulated. Previous models are derived under the assumption that the hand can only rotate around its center of mass [83, 265, 173]. However, the development in this section relax this assumption and allows the formulation of the dynamics of a larger class of rolling tasks [277]. Consider the inertial world fixed frame $\mathcal{W}$, which is without loss of generality attached to the holder where the hand is actuated (*i.e.*, the center of rotation of the hand).

At least locally, the shapes should be of class $\mathcal{C}^2$. Any point of the hand shape is given by the chart $\mathbf{c}_h^h(s_h) = \begin{bmatrix} u_h(s_h) & v_h(s_h) \end{bmatrix}^T \in \mathbb{R}^2$, expressed with respect to $\mathcal{H}$, while any point of the object shape is given by $\mathbf{c}_o^o(s_o) = \begin{bmatrix} u_o(s_o) & v_o(s_o) \end{bmatrix}^T \in \mathbb{R}^2$, expressed with respect to $\mathcal{O}$. Notice that

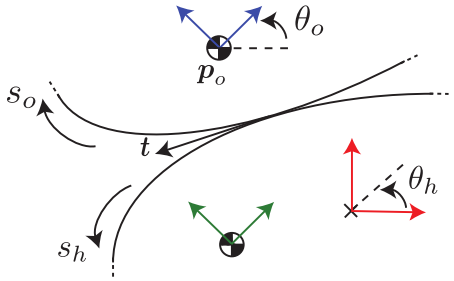

Fig. 6.1: A general nonprehensile planar rolling manipulation system with the center of rotation of the hand (indicated by the $\times$ symbol) not corresponding to its center of mass. The world fixed frame $\mathcal{W}$ is in red. The hand frame $\mathcal{H}$ and the object frame $\mathcal{O}$, in green and blue, respectively, are placed at their respective CoM.

s_h increases counterclockwise along the hand, while s_o increases clockwise along the object. With this choice, the pure rolling assumption is $\dot{s}_h = \dot{s}_o$. Without loss of generality, the frames $\mathcal{W}$ and $\mathcal{H}$ coincide at $\theta_h = 0$, the point $s_h = 0$ is at the intersection between the vertical (gravitational) axis of $\mathcal{W}$ and the hand shape (*i.e.*, $\mathbf{c}_h(0) = \begin{bmatrix} 0 & v_h(0) \end{bmatrix}^T$ in $\mathcal{W}$), and thus $s_h = s_o$ at all times during rolling. Therefore, the contact location will be specified only by s_h throughout the remainder of the paper. As the first assumption, the hand and the object maintain pure rolling contact for all time. The arclength parametrization implies the property $\|\mathbf{c}_h^{h\prime}\| = 1$, with the symbol $'$ indicating the derivative with respect to the parameter s_h. The same holds for $\mathbf{c}_o^o(s_h)$. At the contact point $\mathbf{c}_h^h(s_h)$, the tangent vector to the shapes is expressed as $\mathbf{t}^h(s_h) = \mathbf{c}_h^{h\prime} \in \mathbb{R}^2$ forming an angle $\phi_h(s_h) = \text{atan2}(v_h'(s_h), u_h'(s_h))$ in $\mathcal{H}$. The same tangent can be expressed with respect to $\mathcal{O}$ with an angle $\phi_o(s_h) = \text{atan2}(v_o'(s_h), u_o'(s_h))$. The signed curvatures of the shapes are defined as: $\kappa_h(s_h) = \phi_h'(s_h) = u_h'(s_h)v_h''(s_h) - u_h''(s_h)v_h'(s_h)$, $\kappa_o(s_h) = \phi_o'(s_h) = u_o'(s_h)v_o''(s_h) - u_o''(s_h)v_o'(s_h)$. The relative curvature at the contact point is given by

$$\kappa_r(s_h) = \kappa_h(s_h) - \kappa_o(s_h). \tag{6.1}$$

Notice that $\kappa_h(s_h) > 0$ and $\kappa_o(s_h) < 0$ denote convexity at the contact point for the hand and the object, respectively. Hence, $\kappa_r(s_h) > 0$ guarantees a single contact point at least locally [265]. The following constraint expresses the angle of the tangent $\mathbf{t}^h(s_h)$ with respect to $\mathcal{W}$: $\theta_h + \phi_h(s_h) = \theta_o + \phi_o(s_h)$. Therefore, taking into account (6.1), the following relations hold

$$\theta_o = \theta_h + \phi_h(s_h) - \phi_o(s_h), \tag{6.2a}$$

$$\dot{\theta}_o = \dot{\theta}_h + \kappa_r(s_h)\dot{s}_h. \tag{6.2b}$$

Assuming that $\mathbf{R}(\theta) \in SO(2)$ is the rotation matrix in the 2D space, notice that the relation $\dot{\mathbf{R}}(\theta) = \mathbf{R}(\bar{\theta})\dot{\theta}$ holds with $\bar{\theta} = \theta + \frac{\pi}{2}$. The position of the CoM of the hand in $\mathcal{W}$ is denoted by $\mathbf{p}_h(\theta_h) = \begin{bmatrix} u_w(\theta_h) & v_w(\theta_h) \end{bmatrix}^T$. The coincidence between the contact points on both the hand and the object is expressed by $\mathbf{p}_h(\theta_h) + \mathbf{R}(\theta_h)\mathbf{c}_h^h(s_h) = \mathbf{p}_o + \mathbf{R}(\theta_o)\mathbf{c}_o^o(s_h)$, yielding to the equation $\mathbf{p}_o = \mathbf{p}_h(\theta_h) + \mathbf{R}(\theta_h)\mathbf{c}_h^h(s_h) - \mathbf{R}(\theta_o)\mathbf{c}_o^o(s_h)$, and, consequently, $\dot{\mathbf{p}}_o = \boldsymbol{\gamma}(\mathbf{q})\dot{\theta}_h + \boldsymbol{\eta}(\mathbf{q})\dot{s}_h = \begin{bmatrix} \boldsymbol{\gamma}(\mathbf{q}) & \boldsymbol{\eta}(\mathbf{q}) \end{bmatrix} \dot{\mathbf{q}}$, with $\mathbf{q} = \begin{bmatrix} \theta_h & s_h \end{bmatrix}^T$ and

$$\boldsymbol{\gamma} = \mathbf{p}_h^{\backprime} + \mathbf{R}(\bar{\theta}_h)\mathbf{c}_h^h - \mathbf{R}(\bar{\theta}_o)\mathbf{c}_o^o, \tag{6.3a}$$

$$\boldsymbol{\eta} = \mathbf{R}(\theta_h)\mathbf{c}_h^{h\prime} - \mathbf{R}(\theta_o)\mathbf{c}_o^{o\prime} - \kappa_r\mathbf{R}(\bar{\theta}_o)\mathbf{c}_o^o, \tag{6.3b}$$

in which dependencies have been dropped, while (6.2b) is included and (6.2a) has to be plugged in. The symbol $^{\backprime}$ indicates the derivative with respect to θ_h. For this class of systems the kinetic energy is given by

$$T = \frac{1}{2}\left(I_h\dot{\theta}_h^2 + m_h\dot{\mathbf{p}}_h^T(\theta_h)\dot{\mathbf{p}}_h(\theta_h) + m_o\dot{\mathbf{p}}_o^T\dot{\mathbf{p}}_o + I_o\dot{\theta}_o^2\right) = \frac{1}{2}\mathbf{p}^T\mathbf{M}^{-1}(\mathbf{q})\mathbf{p},$$

where the elements of the mass matrix are given by $m_{11}(\mathbf{q}) = I_h + I_o + m_h\mathbf{p}_h^{\backprime T}\mathbf{p}_h^{\backprime} + m_o\boldsymbol{\gamma}^T(\mathbf{q})\boldsymbol{\gamma}(\mathbf{q})$, $m_{12}(\mathbf{q}) = I_o\kappa_r(s_h) + m_o\boldsymbol{\gamma}(\mathbf{q})^T\boldsymbol{\eta}(\mathbf{q})$, and $m_{22}(\mathbf{q}) = I_o\kappa_r^2(s_h) + m_o\boldsymbol{\eta}(\mathbf{q})^T\boldsymbol{\eta}(\mathbf{q})$. The potential energy is, instead, given by

$$V(\mathbf{q}) = g\mathbf{e}_2^T(m_o\mathbf{p}_o(\mathbf{q}) + m_h\mathbf{p}_h(\mathbf{q})). \tag{6.4}$$

Given the kinetic and potential energy functions, then the dynamics of a mechanical system can be readily derived using the Euler-Lagrange equations or equivalently the Hamilton canonical equation of motion [160].

6.3 Input-state feedback linearisation

The scope of this section is to find and apply a general diffeomorphism to achieve an input-state FLin of the whole dynamics. Such state transformation renders the system in the so-called *normal form* (i.e., a chain of integrators) without internal dynamics. Given some assumptions on the shapes of both the object and the hand, EFL is employed to stabilize the system.

For a brief mathematical background regarding input-state linearisation and differential flatness, please see [173].

6.3.1 Hypotheses on the shapes and input-state linearisation

Having in mind the derivation in Section 6.2, the dynamic model is derived through the *Euler-Lagrange* formalism. The so-called Lagrange function is given by $\mathcal{L} = T - V$. The dynamic model equations are then given by $\frac{\mathrm{d}}{\mathrm{d}t}\frac{\partial \mathcal{L}}{\partial \dot{q}_i} - \frac{\partial \mathcal{L}}{\partial q_i} = \tau_i$, with $i = 1, 2$ and τ_i the associated generalized force acting on the ith generalized coordinate. Therefore, by computing the Lagrange equations and considering the Christoffel symbols of the first type [284], the dynamic model can be written as $\mathbf{M}(\mathbf{q})\ddot{\mathbf{q}} + \mathbf{C}(\mathbf{q}, \dot{\mathbf{q}})\dot{\mathbf{q}} + \mathbf{g}(\mathbf{q}) = \boldsymbol{\tau}$, where $\boldsymbol{\tau} = \begin{bmatrix} \tau_h & 0 \end{bmatrix}^T$ represents the generalized input force, $\mathbf{g}(\mathbf{q}) = \left(\frac{\partial \mathcal{V}(\mathbf{q})}{\partial \mathbf{q}}\right)^T$, and $\mathbf{C}(\mathbf{q}, \dot{\mathbf{q}})$ is a suitable matrix whose generic element is given by

$$c_{ij}(\mathbf{q}, \dot{\mathbf{q}}) = \frac{1}{2}\sum_{k=1}^{2}\left(\frac{\partial m_{ij}(\mathbf{q})}{\partial q_k} + \frac{\partial m_{ik}(\mathbf{q})}{\partial q_j} - \frac{\partial m_{jk}(\mathbf{q})}{\partial q_i}\right)\dot{q}_k, \tag{6.5}$$

with $i, j = 1, 2$. By neglecting dependencies, the dynamic model can be written in the following extended form

$$m_{11}\ddot{\theta}_h + m_{12}\ddot{s}_h + c_{11}\dot{\theta}_h + c_{12}\dot{s}_h + g_1 = \tau_h, \tag{6.6a}$$
$$m_{12}\ddot{\theta}_h + m_{22}\ddot{s}_h + c_{21}\dot{\theta}_h + c_{22}\dot{s}_h + g_2 = 0. \tag{6.6b}$$

During experimentation, when highly-geared harmonic drive plus DC motors are present, the hand's angular acceleration is more convenient than the hand's torque [265]. It is thus suitable to rewrite (6.6) with $\ddot{\theta}_h = a_h$ as input

$$\ddot{\theta}_h = a_h, \tag{6.7a}$$
$$\ddot{s}_h = -m_{22}^{-1}(m_{12}a_h + c_{21}\dot{\theta}_h + c_{22}\dot{s}_h + g_2), \tag{6.7b}$$

where dependencies have been neglected. The equation relating τ_h and a_h is given by

$$\tau_h = \xi(\mathbf{q}, \dot{\mathbf{q}}) + \sigma(\mathbf{q})a_h, \tag{6.8}$$

with $\xi(\mathbf{q}, \dot{\mathbf{q}}) = g_1 + c_{11}\dot{\theta}_h + c_{12}\dot{s}_h - \frac{m_{12}}{m_{22}}(g_2 + c_{21}\dot{\theta}_h + c_{22}\dot{s}_h)$ and $\sigma(\mathbf{q}) = m_{11} - \frac{m_{12}^2}{m_{22}}$.

Assumption 6.3.1 The Coriolis terms $c_{21}(\mathbf{q}, \dot{\mathbf{q}})$ and $c_{22}(\mathbf{q}, \dot{\mathbf{q}})$ are equal to zero. □

Remark 6.3.1 Looking at (6.5), Assumption 6.3.1 is verified when terms $m_{12} = m_{21}$ and m_{22} do not depend on $\mathbf{q}$, and when m_{11} depends only on θ_h. Looking at the particular expressions of m_{ij}, this means that κ_r has to be constant, *i.e.* $\kappa_r' = 0$, the combination of the products $\boldsymbol{\gamma}(\mathbf{q})^T\boldsymbol{\eta}(\mathbf{q})$ and $\boldsymbol{\eta}(\mathbf{q})^T\boldsymbol{\eta}(\mathbf{q})$ do not depend on $\mathbf{q}$, and the product $\boldsymbol{\gamma}(\mathbf{q})^T\boldsymbol{\gamma}(\mathbf{q})$ depends only on θ_h. Considering (6.3) and the expressions of $\kappa_h(s_h)$ and $\kappa_o(s_h)$, the aforementioned properties are thus governed by the shapes of both the hand and the object. □

Assumption 6.3.1 simplifies (6.7) as follows

$$\ddot{\theta}_h = a_h, \tag{6.9a}$$

$$\ddot{s}_h = -\frac{1}{m_{22}}(m12a_h + g_2(\mathbf{q})). \tag{6.9b}$$

By indicating the state of the system as $\mathbf{x} = \begin{bmatrix} x_1 & x_2 & x_3 & x_4 \end{bmatrix}^T = \begin{bmatrix} \theta_h & \dot{\theta}_h & s_h & \dot{s}_h \end{bmatrix}^T \in \mathbb{R}^4$, (6.9) can be written in the affine state-space form $\dot{\mathbf{x}} = \mathbf{f}(\mathbf{x}) + \mathbf{b}(\mathbf{x})u$, with $u = a_h$ and

$$\mathbf{f}(\mathbf{x}) = \begin{bmatrix} x_2 & 0 & x_4 & -\dfrac{g_2(\mathbf{x})}{m_{22}} \end{bmatrix}^T \in \mathbb{R}^4, \tag{6.10a}$$

$$\mathbf{b} = \begin{bmatrix} 0 & 1 & 0 & -\dfrac{m_{12}}{m_{22}} \end{bmatrix}^T \in \mathbb{R}^4. \tag{6.10b}$$

In order to check whether (6.9) is input-state FLin, the controllability matrix $\mathbf{T}(\mathbf{x}) = \begin{bmatrix} \mathbf{b} & \mathrm{ad}_{\mathbf{f}}\mathbf{b} & \mathrm{ad}_{\mathbf{f}}^2\mathbf{b} & \mathrm{ad}_{\mathbf{f}}^3\mathbf{b} \end{bmatrix} \in \mathbb{R}^{4\times 4}$ has to be invertible in a certain region Ω, and the set given by the first three columns of $\mathbf{T}(\mathbf{x})$ has to be involutive. Taking into account (6.10), the detailed expression of the controllability matrix is

$$\mathbf{T}(\mathbf{x}) = \begin{bmatrix} 0 & -1 & 0 & 0 \\ 1 & 0 & 0 & 0 \\ 0 & \dfrac{m_{21}}{m_{22}} & 0 & t_{34} \\ -\dfrac{m_{21}}{b_{22}} & 0 & t_{43} & t_{44} \end{bmatrix}, \tag{6.11}$$

with $t_{34} = \dfrac{1}{m_{22}}\dfrac{\partial g_2(\mathbf{x})}{\partial x_1} - \dfrac{m_{12}}{m_{22}^2}\dfrac{\partial g_2(\mathbf{x})}{\partial x_3}$, $t_{43} = \dfrac{m_{12}}{m_{22}^2}\dfrac{\partial g_2(\mathbf{x})}{\partial x_3} - \dfrac{1}{m_{22}}\dfrac{\partial g_2(\mathbf{x})}{\partial x_1}$, and $t_{44} = x_4\dfrac{m_{12}}{m_{22}}\dfrac{\partial^2 g_2(\mathbf{x})}{\partial x_3^2} - \dfrac{x_2}{m_{22}}\dfrac{\partial^2 g_2(\mathbf{x})}{\partial x_1^2}$. Defining the region $\Omega = \left\{\mathbf{x} \in \mathbb{R}^4 : \dfrac{\partial g_2(\mathbf{x})}{\partial x_1} \neq \dfrac{m_{12}}{m_{22}}\dfrac{\partial g_2(\mathbf{x})}{\partial x_3}\right\}$, it is possible to prove that $\mathbf{T}(\mathbf{x})$ in (6.11) is made by linearly independent columns: the first three of them build an involutive set (proofs are omitted for brevity). The system (6.9) is then input-state FLin in Ω.

To bring (6.9) in the following normal form

$$\begin{cases} \dot{z}_i = z_{i+1} \\ \dot{z}_n = v \end{cases}, \tag{6.12}$$

with $i = 1, \ldots, n-1$, and $v \in \mathbb{R}$ and $z_i \in \mathbb{R}$ a new input and state variable, respectively, a diffeomorphism

$$\mathbf{z} = \begin{bmatrix} z_1 & z_2 & \cdots & z_n \end{bmatrix}^T = \boldsymbol{\phi}(\mathbf{x}) = \begin{bmatrix} z_1 & L_{\mathbf{f}} z_1 & \ldots & L_{\mathbf{f}}^{n-1} z_1 \end{bmatrix}^T \tag{6.13}$$

has to be found. Hence, in order to compute the first component z_1, the following equations

$$\frac{\partial z_1}{\partial \mathbf{x}} \mathrm{ad}_{\mathbf{f}}^i \mathbf{b} = 0, \tag{6.14a}$$

$$\frac{\partial z_1}{\partial \mathbf{x}} \mathrm{ad}_{\mathbf{f}}^{n-1} \mathbf{b} \neq 0, \tag{6.14b}$$

with $i = 0, \ldots, n-2$, must hold for the vector fields (6.10). In particular, looking at the expression of the first three columns of $\mathbf{T}(\mathbf{x})$, condition (6.14a) yields $\dfrac{\partial z_1}{\partial x_2} - \dfrac{m_{12}}{m_{22}} \dfrac{\partial z_1}{\partial x_4} = 0$, $\dfrac{m_{12}}{m_{22}} \dfrac{\partial z_1}{\partial x_3} - \dfrac{\partial z_1}{\partial x_1} = 0$, and $\dfrac{\partial z_1}{\partial x_4} t_{43} = 0$. The solution to this system is then given by $z_1 = \dfrac{m_{12}}{m_{22}} x_1 + x_3$. It is easy to verify that such a choice for z_1 also satisfies (6.14b). Therefore, the complete diffeomorphism is given by

$$\boldsymbol{\phi}(\mathbf{x}) = \begin{bmatrix} z_1 \\ z_2 \\ z_3 \\ z_4 \end{bmatrix} = \begin{bmatrix} y \\ \dot{y} \\ \ddot{y} \\ y^{(3)} \end{bmatrix} = \begin{bmatrix} \dfrac{m_{12}}{m_{22}} x_1 + x_3 \\ \dfrac{m_{12}}{m_{22}} x_2 + x_4 \\ -\dfrac{g_2(\mathbf{x})}{m_{22}} \\ -\dfrac{1}{m_{22}} \left(\dfrac{\partial g_2(\mathbf{x})}{\partial x_1} x_2 + \dfrac{\partial g_2(\mathbf{x})}{\partial x_3} x_4 \right) \end{bmatrix}, \tag{6.15}$$

where $y^{(j)}$ is the jth-order derivative, with $j \geq 3$. The input transformation $a_h = \alpha(\mathbf{x}) + \beta(\mathbf{x}) v$ finally renders (6.9) in the normal form (6.12), with

$$\alpha(\mathbf{x}) = -\frac{\left(\dfrac{\partial^2 g_2(\mathbf{x})}{\partial x_1^2}x_2 - \dfrac{g_2(\mathbf{x})}{m_{22}}\dfrac{\partial g_2(\mathbf{x})}{\partial x_3} + \dfrac{\partial^2 g_2(\mathbf{x})}{\partial x_3^2}x_4\right)}{\left(\dfrac{\partial g_2(\mathbf{x})}{\partial x_1} - \dfrac{m_{12}}{m_{22}}\dfrac{\partial g_2(\mathbf{x})}{\partial x_3}\right)}, \tag{6.16a}$$

$$\beta(\mathbf{x}) = -m_{22}\left(\frac{\partial g_2(\mathbf{x})}{\partial x_1} - \frac{m_{12}}{m_{22}}\frac{\partial g_2(\mathbf{x})}{\partial x_3}\right)^{-1}. \tag{6.16b}$$

This is the core result since, under Assumption 6.3.1, a general diffeomorphism is found to change a nonprehensile 2D rolling manipulation system into a normal form where simple linear controllers can be applied.

Therefore, in general, any suitable approach can be employed to control the normal form (6.12). The EFL technique [120] is here considered . In detail, a change of coordinates is applied to (6.9) through (6.15). To get the normal form, the EFL technique does not use the feedback transformation $a_h = \alpha(\mathbf{x}) + \beta(\mathbf{x})v$, but $a_h = \alpha(\mathbf{x}^\star) + \beta(\mathbf{x}^\star)v$, where $\mathbf{x}^\star$ is the desired state[1] (in feedforward). The new virtual input v is instead designed as an extended PID^{n-1} plus a feedforward action

$$v = z_4^\star + \sum_{i=0}^{4} k_i e_i, \tag{6.17a}$$

$$e_0 = \int_o^t e_1(\tau)\mathrm{d}\tau, \tag{6.17b}$$

$$e_i = z_i^\star - z_i, \tag{6.17c}$$

with k_i positive gains such that the resulting characteristic polynomial is Hurwitz.

6.3.2 Case studies

6.3.2.1 Disk-on-disk

This case study considers the balancing of a disk free to roll on an actuated disk. Referring to Fig. 6.2, the shape of the hand, *i.e.* the actuated disk, is parametrized by $\mathbf{c}_h^h(s_h) = \rho_h\left[-\sin\dfrac{s_h}{\rho_h} \;\; \cos\dfrac{s_h}{\rho_h}\right]^T$. The upper disk's shape is parametrized by $\mathbf{c}_o^o(s_h) = -\rho_o\left[\sin\dfrac{s_h}{\rho_o} \;\; \cos\dfrac{s_h}{\rho_o}\right]^T$. Considering (6.1), the relative curvature is given by $\kappa_r = \dfrac{\rho_h + \rho_o}{\rho_h\rho_o}$. The upper disk angular

[1] Eventually retrieved from $\mathbf{z}^\star$ through $\boldsymbol{\phi}^{-1}$.

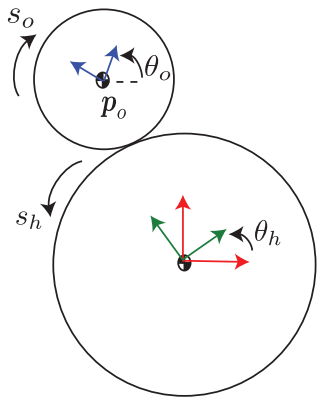

Fig. 6.2: A representation of the DoD system. In red the world fixed frame $\mathcal{W}$. In green the hand frame $\mathcal{H}$, while in blue the object frame $\mathcal{O}$, placed at the respective CoMs .

velocity is given by $\dot{\theta}_o = \dot{\theta}_h + \kappa_r \dot{s}_h$. The vectors $\boldsymbol{\gamma}(\mathbf{q})$ and $\boldsymbol{\eta}(\mathbf{q})$ are computed like in (6.3): $\boldsymbol{\gamma}(\mathbf{q}) = -(\rho_h+\rho_o)\left[\cos\left(\theta_h + \frac{s_h}{\rho_h}\right) \;\; \sin\left(\theta_h + \frac{s_h}{\rho_h}\right)\right]^T$, and $\boldsymbol{\eta}(\mathbf{q}) = -\rho_o\kappa_r\left[\cos\left(\theta_h + \frac{s_h}{\rho_h}\right) \;\; \sin\left(\theta_h + \frac{s_h}{\rho_h}\right)\right]^T$. Therefore, the parameters of the DoD dynamic model are $m_{11} = I_h + I_o + m_o(\rho_h + \rho_o)^2$, $m_{12} = m_{21} = I_o\kappa_r + m_o\frac{(\rho_h+\rho_o)^2}{\rho_h}$, $m_{22} = I_o\kappa_r^2 + m_o\rho_o^2\kappa_r^2$, $c_{11} = c_{12} = c_{21} = c_{22} = 0$, $g_1 = -m_o g(\rho_h + \rho_o)\sin\left(\theta_h + \frac{s_h}{\rho_h}\right)$ and $g_2 = -m_o g\rho_o\kappa_r \sin\left(\theta_h + \frac{s_h}{\rho_h}\right)$. Notice that the quantity $\theta_h + \frac{s_h}{\rho_h}$ is the angle of the object's CoM with respect to the vertical axis of $\mathcal{W}$. It is possible to verify that the DoD dynamic model fully verifies Assumption 6.3.1. Hence, considering the acceleration a_h of the actuated disk as input, the DoD dynamics can be written as in (6.9) with τ_h as in (6.8). The affine state space form assumes the following vector fields (6.10) $\mathbf{f}(\mathbf{x}) = \left[x_2 \;\; 0 \;\; x_4 \;\; \frac{m_o g\rho_o \sin\left(x_1 + \frac{x_3}{\rho_h}\right)}{I_o\kappa_r + m_o\rho_o^2\kappa_r}\right]^T$ and $\mathbf{b} = \left[0 \;\; 1 \;\; 0 \;\; -\frac{m_o\rho_o^2 + m_o\rho_h\rho_o + I_o}{\kappa_r(m_o\rho_o^2 + I_o)}\right]^T$. Computing the matrix $\mathbf{T}(\mathbf{x})$ as in (6.11), it is possible to verify that the approximate dynamic model is input-state linearizable in the region $\Omega = \left\{\mathbf{x} \in \mathbb{R}^4 : \cos\left(x_1 + \frac{x_3}{\rho_h}\right) \neq 0 \Rightarrow |x_1 + \frac{x_3}{\rho_h}| < \frac{\pi}{2}\right\}$. Notice that such a region is not restrictive because, with no bound on other states, Ω covers all practical situations since outside it the disk falls down

from the hand. Finally, the diffeomorphism (6.15) is

$$\phi(\mathbf{x}) = \Bigg[\frac{m_{12}}{m_{22}}x_1 + x_3 \quad \frac{m_{12}}{m_{22}}x_2 + x_4 \quad \frac{m_o g \rho_o \sin\left(x_1 + \frac{x_3}{\rho_h}\right)}{I_o\kappa_r + m_o\rho_o^2\kappa_r} \quad \frac{m_o g \rho_o \kappa_r \left(x_2 + \frac{x_4}{\rho_h}\right)\cos\left(x_1 + \frac{x_3}{\rho_h}\right)}{b_{22}}\Bigg]^T,$$

with

$$\alpha(\mathbf{x}) = \frac{\sin\left(x_1 + \frac{x_3}{\rho_h}\right)x_2 - \left(\frac{m_o g \rho_o \kappa_r}{b_{22}\rho_h}\sin\left(x_1 + \frac{x_3}{\rho_h}\right) + \frac{x_4}{\rho_h^2}\right)\cos\left(x_1 + \frac{x_3}{\rho_h}\right)}{\left(1 - \frac{b_{12}}{b_{22}\rho_h}\right)\cos\left(x_1 + \frac{x_3}{\rho_h}\right)}$$

and $\beta(\mathbf{x}) = m_{22}\left(m_o g \rho_o \kappa_r \left(1 - \frac{m_{12}}{m_{22}\rho_h}\right)\cos\left(x_1 + \frac{x_3}{\rho_3}\right)\right)^{-1}$. The control is again performed with the EFL technique described in Section 6.3.1.

Remark 6.3.2 Notice that in this case study the only possibility of balancing is with the object directly above the hand's CoM, *i.e.* $\theta_h + \frac{s_h}{\rho_h} = 0$. As noticed in [265], any other balancing position leads to constant angular acceleration resulting in unbounded velocities.The differential flatness loses thus some sense for the disk on disk. □

Looking at $\boldsymbol{\phi}(\mathbf{x})$, stabilizing the origin $\mathbf{z} = \mathbf{0_4}$ is equivalent to stabilizing $\mathbf{x} = \mathbf{0_4}$ and then $x_1 + \frac{x_3}{\rho_h} = 0$. However, notice that through the following further change of coordinates $\bar{\mathbf{z}} = \left[z_1 - \left(\frac{m_{12} - m_{22}\rho_h}{m_{22}}\theta_h^\star\right) \;\; z_2 \;\; z_3 \;\; z_4\right]^T \in \mathbb{R}^4$ it is possible to balance the object with θ_h at a desired constant angle $\theta_h^\star = x_1^\star$. It is easy to verify that such additional diffeomorphism does not change the normal form (6.12) expressed now in terms of $\bar{\mathbf{z}}$. With some algebra, it is possible to show that stabilizing the origin $\bar{\mathbf{z}} = \mathbf{0_4}$ yields $x_1 = x_1^\star$, $x_1 + \frac{x_3}{\rho_h} = 0$ and $x_2 = x_4 = 0$.

The input-state FLin plus the EFL controller are employed in [173] on a real-hardware DoD device.

6.3.2.2 Ball-and-beam

Referring to Fig. 6.3, the beam can rotate around its center of mass while the ball can only roll along the beam. The shape of the hand, *i.e.*, the beam, is parametrized through $\mathbf{c}_h^h(s_h) = \begin{bmatrix}-s_h & d_h\end{bmatrix}^T$. The ball's shape is

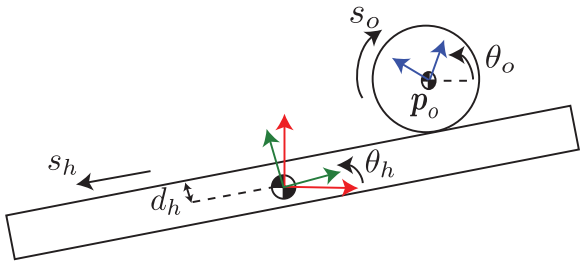

Fig. 6.3: A representation of the BnB system. In red the world fixed frame $\mathcal{W}$. In green the hand frame $\mathcal{H}$, while in blue the object frame $\mathcal{O}$, placed at the respective CoMs.

parametrized by $\mathbf{c}_o^o(s_h) = -\rho_o \left[\sin\frac{s_h}{\rho_o} \;\; \cos\frac{s_h}{\rho_o}\right]^T$. Considering (6.1), the signed curvatures of the beam and the ball are $\kappa_h = 0$ and $\kappa_o = \rho_o^{-1}$, respectively. The relative curvature is thus given by $\kappa_r = \rho_o^{-1}$. The ball's angular velocity is instead given by (6.2b) $\dot{\theta}_o = \dot{\theta}_h + \frac{\dot{s}_h}{\rho_o}$. In order to compute the mass matrix of the system, the vectors $\boldsymbol{\gamma}(\mathbf{q})$ and $\boldsymbol{\eta}(\mathbf{q})$ in (6.3) are $\boldsymbol{\gamma}(\mathbf{q}) = \left[-(\rho_o + d_h)\cos\theta_h + s_h \sin\theta_h \;\; -(\rho_o + d_h)\sin\theta_h - s_h\cos\theta_h\right]^T$, and $\boldsymbol{\eta}(\mathbf{q}) = \left[-\cos(\theta_h) \;\; -\sin(\theta_h)\right]^T$. Therefore, the parameters of the BnB dynamic model are $m_{11} = I_h + I_o + m_o d_h^2 + 2m_o d_h \rho_o + m_o \rho_o^2 + m_o s_h^2$, $m_{12} = m_{21} = \frac{I_o}{\rho_o} + m_o d_h + m_o \rho_o$, $m_{22} = \frac{I_o}{\rho_o^2} + m_o$, $c_{11} = m_o s_h \dot{s}_h$, $c_{12} = m_o s_h \dot{\theta}_h$, $c_{21} = m_o s_h \dot{\theta}_h$, $c_{22} = 0$, $g_1 = -m_o g((d_h + \rho_o)\sin\theta_h + s_h \cos\theta_h)$ and $g_2 = -m_o g \sin\theta_h$. Considering the acceleration a_h of the beam as input, the system can be written as in (6.7), with τ_h as in (6.8). However, it is possible to verify that Assumption 6.3.1 is not verified for the ball and beam case since $c_{21} \neq 0$. Even if κ_r is constant and the products $\boldsymbol{\gamma}(\mathbf{q})^T\boldsymbol{\eta}(\mathbf{q})$ and $\boldsymbol{\eta}(\mathbf{q})^T\boldsymbol{\eta}(\mathbf{q})$ do not depend on $\mathbf{q}$, the product $\boldsymbol{\gamma}(\mathbf{q})^T\boldsymbol{\gamma}(\mathbf{q})$ does not depend only on θ_h, but it depends on the arclength parameter. Therefore, the ball and beam system is not input-state linearizable. This result is well known in the literature, nevertheless, in many cases it is possible to approximate c_{21} to zero [127]. This is true for small velocities of the beam, small masses of the ball and not so long beam. Hence, by putting $c_{21} = 0$, only for control design purposes, it is possible to write the approximated ball and beam system like in (6.9). The affine state space form of the approximated ball and beam system has the following vector fields (6.10) $\mathbf{f}(\mathbf{x}) = \left[x_2 \;\; 0 \;\; x_4 \;\; \frac{m_o \rho_o^2 g \sin x_1}{I_o + m_o \rho_o^2}\right]^T$ and $\mathbf{b} = \left[0 \;\; 1 \;\; 0 \;\; -\rho_o \frac{m_o \rho_o^2 + d_h m_o \rho_o + I_o}{I_o + m_o \rho_o^2}\right]^T$. Computing the matrix $\mathbf{T}(\mathbf{x})$ as in (6.11), it is possible to verify that the approximate dynamic model is

input-state FLin in the region $\Omega = \left\{\mathbf{x} \in \mathbb{R}^4 : \cos\theta_h \neq 0 \Rightarrow |\theta_h| < \frac{\pi}{2}\right\}$. Notice that such a region is not restrictive because, with no bound on other states, Ω covers all practical situations since outside it the ball falls down from the hand. Finally, it is possible to compute the diffeomorphism (6.15) $\boldsymbol{\phi}(\mathbf{x}) = \left[\frac{m_{12}}{m_{22}}x_1 + x_3 \;\; \frac{m_{12}}{m_{22}}x_2 + x_4 \;\; \frac{m_o g}{b_{22}}\sin x_1 \;\; \frac{m_o g x_2}{m_{22}}\cos x_1\right]^T$, yielding the normal form

$$\dot{z}_1 = z_2, \tag{6.18a}$$
$$\dot{z}_2 = z_3, \tag{6.18b}$$
$$\dot{z}_3 = z_4, \tag{6.18c}$$
$$\dot{z}_4 = \beta(\mathbf{x})|^{-1}_{\mathbf{x}=\boldsymbol{\phi}^{-1}(\mathbf{z})}\left(a_h - \alpha(\mathbf{x})|_{\mathbf{x}=\boldsymbol{\phi}^{-1}(\mathbf{z})}\right), \tag{6.18d}$$

with $\alpha(\mathbf{x}) = m_o g x_2 \tan x_1$ and $\beta(\mathbf{x}) = \dfrac{m_{22}}{m_o g \cos x_1}$ from (6.16). The control is then performed with the EFL technique described in Section 6.3.1.

The designed controller for the BnB system is tested in simulation within [173], showing acceptable performance despite the employed assumption to make the BnB system as input-state feedback linearisable.

6.4 Passivity-based approach

6.4.1 Background on passivity-based control

6.4.1.1 Port-Hamiltonian systems

The pH framework allows modeling of mechanical systems including the information about the energy transfer explicitly. The canonical Hamiltonian equations of motion are

$$\begin{bmatrix}\dot{\mathbf{q}}\\ \dot{\mathbf{p}}\end{bmatrix} = \begin{bmatrix}\mathbf{O}_2 & \mathbf{I}_2\\ -\mathbf{I}_2 & \mathbf{O}_2\end{bmatrix}\nabla H(\mathbf{q},\mathbf{p}) + \begin{bmatrix}\mathbf{0}_2\\ \mathbf{g}_i(\mathbf{q})\end{bmatrix}u, \tag{6.19}$$

where $\mathbf{g}_i(\mathbf{q}) \in \mathbb{R}^2$ is the input mapping vector. The function H is the Hamiltonian, which represents the total energy (kinetic plus potential) stored in the system, having the form

$$H(\mathbf{q},\mathbf{p}) = \frac{1}{2}\mathbf{p}^T\mathbf{M}^{-1}(\mathbf{q})\mathbf{p} + V(\mathbf{q}).$$

A full development of the Hamilton canonical equations of motion can be found in [160].

6.4.1.2 Interconnection and damping assignment

The stabilisation problem of the dynamics (6.19) to the desired equilibrium $(\mathbf{q}, \mathbf{p}) = (\mathbf{q}^\star, \mathbf{0}_2)$ is achieved using the IDA-PBC by assigning the target dynamics to the closed loop [236]

$$\begin{bmatrix} \dot{\mathbf{q}} \\ \dot{\mathbf{p}} \end{bmatrix} = \begin{bmatrix} \mathbf{O}_2 & \mathbf{M}^{-1}(\mathbf{q})\mathbf{M}_d(\mathbf{q}) \\ -\mathbf{M}_d(\mathbf{q})\mathbf{M}^{-1}(\mathbf{q}) & \mathbf{J}_2(\mathbf{q}, \mathbf{p}) \end{bmatrix} \nabla H_d(\mathbf{q}, \mathbf{p}), \tag{6.20}$$

where $\mathbf{J}_2(\mathbf{q}, \mathbf{p}) \in \mathbb{R}^{2\times 2}$ is the desired interconnection matrix. The desired total energy function is given by

$$H_d(\mathbf{q}, \mathbf{p}) = \frac{1}{2}\mathbf{p}^T\mathbf{M}_d^{-1}(\mathbf{q})\mathbf{p} + V_d(\mathbf{q}), \tag{6.21}$$

with $V_d(\mathbf{q}) \in \mathbb{R}$ the desired potential energy function. Then, $(\mathbf{q}^\star, \mathbf{0}_2)$ will be a stable equilibrium configuration of the closed-loop (6.20) if

C.1 $\mathbf{M}_d(\mathbf{q})$ is symmetric and positive definite;
C.2 $\mathbf{q}^\star = \arg\min V_d(\mathbf{q})$;
C.3 $\mathbf{J}_2(\mathbf{q}, \mathbf{p})$ is skew-symmetric.

The stabilization of the desired equilibrium is achieved by identifying the class of Hamiltonian systems that can be obtained via feedback. The conditions under which this feedback law exists are the matching conditions, *i.e.*, matching the original dynamic system (6.19) and the target dynamic system (6.20):

$$\begin{bmatrix} \mathbf{O}_2 & \mathbf{I}_2 \\ -\mathbf{I}_2 & \mathbf{O}_2 \end{bmatrix} \nabla H + \begin{bmatrix} \mathbf{0}_2 \\ \mathbf{g}_i(\mathbf{q}) \end{bmatrix} \mathbf{u} = \begin{bmatrix} \mathbf{0}_2 & \mathbf{M}^{-1}\mathbf{M}_d \\ -\mathbf{M}_d\mathbf{M}^{-1} & \mathbf{J}_2 \end{bmatrix} \nabla H_d, \tag{6.22}$$

where the dependency of the functions on their argument has been drop to simplify the notation. The first line in (6.22) is straightforwardly satisfied, while the second line in (6.22) corresponds to the following set of PDEs

$$\mathbf{g}_i^\perp(\mathbf{q}) \left(\nabla_q H(\mathbf{q}, \mathbf{p}) - \mathbf{M}_d(\mathbf{q})\mathbf{M}^{-1}(\mathbf{q})\nabla_q H_d(\mathbf{q}, \mathbf{p}) + \mathbf{J}_2(\mathbf{q}, \mathbf{p})\mathbf{M}_d^{-1}(\mathbf{q})\mathbf{p} \right) = 0, \tag{6.23}$$

where $\mathbf{g}_i^\perp(\mathbf{q}) \in \mathbb{R}^{1\times 2}$ is the full rank left annihilator of $\mathbf{g}_i(\mathbf{q})$, which satisfies $\mathbf{g}_i^\perp(\mathbf{q})\mathbf{g}_i(\mathbf{q}) = 0$. The PDEs (6.23) can be separated into the two subsets of

PDEs, namely

$$\mathbf{g}_i^{\perp}\left(\nabla_q(\mathbf{p}^T\mathbf{M}^{-1}(\mathbf{q})\mathbf{p}) - \mathbf{M}_d(\mathbf{q})\mathbf{M}^{-1}(\mathbf{q})\nabla_q(\mathbf{p}^T\mathbf{M}_d^{-1}(\mathbf{q})\mathbf{p}) + 2\mathbf{J}_2(\mathbf{q},\mathbf{p})\mathbf{M}_d^{-1}(\mathbf{q})\mathbf{p}\right) = 0, \tag{6.24}$$

$$\mathbf{g}_i^{\perp}\left(\nabla_q V(\mathbf{q}) - \mathbf{M}_d(\mathbf{q})\mathbf{M}^{-1}(\mathbf{q})\nabla_q V_d(\mathbf{q})\right) = 0, \tag{6.25}$$

where (6.24) and (6.25) are the kinetic and the potential energy matching equations, respectively. By solving (6.24)-(6.25) for $\mathbf{M}_d(\mathbf{q})$, $V_d(\mathbf{q})$ and $\mathbf{J}_2(\mathbf{q},\mathbf{p})$, subject to **C.1**, **C.2**, and **C.3**, the energy shaping control is given by

$$u_{es} = (\mathbf{g}_i^T(\mathbf{q})\mathbf{g}_i(\mathbf{q}))^{-1}\mathbf{g}_i^T(\mathbf{q})(\nabla_q H(\mathbf{q},\mathbf{p}) - \mathbf{M}_d(\mathbf{q})\mathbf{M}^{-1}(\mathbf{q})\nabla_q H_d(\mathbf{q},\mathbf{p}) + \mathbf{J}_2(\mathbf{q},\mathbf{p})\mathbf{M}_d^{-1}(\mathbf{q})\mathbf{p}). \tag{6.26}$$

It is worth remarking that not every desired $\mathbf{M}_d(\mathbf{q})$, $V_d(\mathbf{q})$ and $\mathbf{J}_2(\mathbf{q},\mathbf{p})$ can be chosen, but only those solving (6.24)-(6.25) subject to the conditions **C.1**, **C.2**, and **C.3**.

By applying (6.26) to the Hamiltonian dynamics (6.19), the closed-loop target dynamics (6.20) is obtained. Damping aimed at achieving asymptotic stability is then injected through

$$u_{di} = -K_v\mathbf{g}_i^T(\mathbf{q})\nabla_p H_d(\mathbf{q},\mathbf{p}), \tag{6.27}$$

where $K_v > 0$ is a gain. The damping injection (6.27) and the energy shaping control (6.26) are then assembled to generate the IDA-PBC

$$u = u_{es} + u_{di}. \tag{6.28}$$

Therefore, through this adjustment, the closed-loop dynamics (6.20) takes the form

$$\begin{bmatrix}\dot{\mathbf{q}}\\ \dot{\mathbf{p}}\end{bmatrix} = \begin{bmatrix}\mathbf{O}_2 & \mathbf{M}^{-1}(\mathbf{q})\mathbf{M}_d(\mathbf{q})\\ -\mathbf{M}_d(\mathbf{q})\mathbf{M}^{-1}(\mathbf{q}) & \mathbf{J}_2(\mathbf{q},\mathbf{p}) - \mathbf{R}_d(\mathbf{q})\end{bmatrix}\nabla H_d(\mathbf{q},\mathbf{p}), \tag{6.29}$$

where $\mathbf{R}_d(\mathbf{q}) = \mathbf{g}_i(\mathbf{q})K_v\mathbf{g}_i^T(\mathbf{q}) \in \mathbb{R}^{2\times 2}$ is the positive-(semi)definite dissipation matrix [235, 236].

The stability of desired equilibrium is analysed by using the desired Hamiltonian (6.21) as a Lyapunov function and computing its time derivative along the trajectories of the closed-loop dynamics (6.29) as follows

$$\begin{aligned}\dot{H}_d(\mathbf{q},\mathbf{p}) &= \nabla_p H_d^T\dot{\mathbf{p}} + \nabla_q H_d^T\dot{\mathbf{q}}\\ &= -\mathbf{p}^T\mathbf{M}_d^{-1}\mathbf{g}_i K_v\mathbf{g}_i^T\mathbf{M}_d^{-1}\mathbf{p} \le 0,\end{aligned}$$

which ensures stability of the desired equilibrium. Asymptotic stability follows from LaSalle's invariance principle [152], or equivalently from detectability of the signal $\mathbf{y}_d = K_v \mathbf{g}_i^T \mathbf{M}_d^{-1} \mathbf{p}$ [323].

6.4.1.3 Integral control

In many cases, the presence of disturbances deteriorates the control system's performance, or in the worst case, will produce instabilities. A typical scenario in practice is to consider constant disturbances, which account for slow-varying perturbations. The dynamics of the closed-loop (6.29) under the action of a matched disturbance is

$$\begin{bmatrix} \dot{\mathbf{q}} \\ \dot{\mathbf{p}} \end{bmatrix} = \begin{bmatrix} \mathbf{O}_2 & \mathbf{M}^{-1}(\mathbf{q})\mathbf{M}_d(\mathbf{q}) \\ -\mathbf{M}_d(\mathbf{q})\mathbf{M}^{-1}(\mathbf{q}) & \mathbf{J}_2(\mathbf{q},\mathbf{p}) - \mathbf{R}_d(\mathbf{q}) \end{bmatrix} \nabla H_d(\mathbf{q},\mathbf{p}) + \begin{bmatrix} \mathbf{0}_2 \\ \mathbf{g}_i(\mathbf{q}) \end{bmatrix} (v + \delta_d), \tag{6.30}$$

where $\delta_d \in \mathbb{R}$ is the matched constant disturbance considered here and $v \in \mathbb{R}$ is a control input that will be used to compensate for the unknown disturbance. To obtain the dynamics (6.30), the control $u = u_{es} + u_{di} + v$ and the disturbance δ_d are used in (6.19). Notice that the disturbance shifts the equilibrium of the closed loop, defined by zero velocities (equivalently $\mathbf{p} = \mathbf{0}_2$), from the desired equilibrium $\mathbf{q}^\star$ to a new equilibrium $\bar{\mathbf{q}}$, which is the solution of

$$-\mathbf{M}_d(\bar{\mathbf{q}})\mathbf{M}(\bar{\mathbf{q}})^{-1}\nabla_q V_d(\bar{\mathbf{q}}) + \mathbf{g}_i(\bar{\mathbf{q}})\delta_d = \mathbf{0}_2.$$

This shows that the controller does not achieve the control objective in the presence of constant disturbances since $\mathbf{q}$ will not reach the desired value at the steady-state as desired. This motivates the implementation of an outer-loop controller to reject constant unknown disturbances.

In this section, the methodology to design integral-based controllers and enhance the robustness of the energy shaping controller reported in [82] will be introduced. The fundamental idea proposed in [82] is to find a dynamic control law $v(\mathbf{q},\mathbf{p},\zeta)$, where $\zeta \in \mathbb{R}$ is the state of the controller, and a change of coordinates such that the closed-loop dynamics that include the controller state expressed in the new coordinates can be written as a port-Hamiltonian system, thus stability is ensured. The proposed target port-Hamiltonian dynamics in new coordinates $\mathbf{z} \in \mathbb{R}^5$, where the state vector has been augmented by adding the controller state. The target port-Hamiltonian system is

$$\begin{bmatrix} \dot{\mathbf{z}}_1 \\ \dot{\mathbf{z}}_2 \\ \dot{z}_3 \end{bmatrix} = \begin{bmatrix} -\mathbf{\Gamma}_1 & \mathbf{M}^{-1}\mathbf{M}_d & -\mathbf{\Gamma}_2 \\ -\mathbf{M}_d\mathbf{M}^{-1} & -K_v\mathbf{g}_i\mathbf{g}_i^T & -\mathbf{g}_i K_3 \\ \mathbf{\Gamma}_2^T & K_3\mathbf{g}_i^T & -\Gamma_3 \end{bmatrix} \begin{bmatrix} \nabla_{\mathbf{z}_1} H_z \\ \nabla_{\mathbf{z}_2} H_z \\ \nabla_{z_3} H_z \end{bmatrix}, \tag{6.31}$$

with Hamiltonian

$$H_z(\mathbf{z}) = \frac{1}{2}\mathbf{z}_2^T \mathbf{M}_d^{-1}\mathbf{z}_2 + V_z(\mathbf{z}_1) + \frac{1}{2}K_I(z_3 - z_3^\star)^2, \tag{6.32}$$

where

$$V_z(\mathbf{z}_1) = V_d(\mathbf{q})\Big|_{\mathbf{q}=\mathbf{z}_1}, \tag{6.33}$$

and the gains are equal to

$$\begin{aligned}
&\boldsymbol{\Gamma}_1 \triangleq K_1 \mathbf{M}^{-1}\mathbf{g}_i\mathbf{g}_i^T\mathbf{M}^{-1},\\
&\boldsymbol{\Gamma}_2 \triangleq K_2 \mathbf{M}^{-1}\mathbf{g}_i,\\
&\Gamma_3 \triangleq K_2 K_3 \mathbf{g}_i^T\mathbf{M}_d^{-1}\mathbf{g}_i,\\
&z_3^\star \triangleq K_I^{-1}\left(K_v K_2 \mathbf{g}_i^T\mathbf{M}_d^{-1}\mathbf{g}_i + K_3\right)^{-1}\delta_d,
\end{aligned}$$

where the new coordinates $\mathbf{z} = \psi(\mathbf{q}, \mathbf{p}, \zeta)$ are obtained by the state transformation

$$\mathbf{z}_1 = \mathbf{q}, \tag{6.34}$$

$$\mathbf{z}_2 = \mathbf{p} + K_1\mathbf{g}_i\mathbf{g}_i^T\mathbf{M}^{-1}\nabla V_d(\mathbf{q}) + K_2K_I(\zeta - z_3^\star)\mathbf{g}_i, \tag{6.35}$$

$$z_3 = \zeta, \tag{6.36}$$

with $K_v > 0$, $K_I > 0$, $K_1 > 0$, $K_3 > 0$ and $K_2 = \left(\mathbf{g}_i^T\mathbf{M}_d^{-1}\mathbf{g}_i\right)^{-1}$.

Notice that Hamiltonian H_z in (6.32) has a minimum at $\mathbf{z}^\star = (\mathbf{q}^\star, \mathbf{0}_n, z_3^\star)$, which is the desired equilibrium. Therefore, we look for a control law that render the extended closed-loop dynamics in the form (6.31) to ensure stability of the equilibrium $\mathbf{z}^\star$. As shown in [82], the control law is obtained by matching the dynamics (6.30) and (6.31), and using the change of coordinates (6.34)-(6.36). It is shown that, under a few assumptions on the matrices $\mathbf{M}$, $\mathbf{M}_d$ and $\mathbf{g}_i^T$, the integral controller takes the form

$$\begin{aligned}
v(\mathbf{q},\mathbf{p},\zeta) = &-\Bigg[K_vK_1\mathbf{g}_i^T\mathbf{M}_d^{-1}\mathbf{g}_i\mathbf{g}_i^T\mathbf{M}^{-1} + K_1\mathbf{g}_i^\top\dot{\mathbf{M}}^{-1}\\
&+K_2K_I\Big(K_2 + K_3\mathbf{g}_i^T\mathbf{M}_d^{-1}\mathbf{g}_iK_1\Big)\mathbf{g}_i^T\mathbf{M}^{-1}\Bigg]\nabla V_d\\
&-\Bigg[K_1\mathbf{g}_i^T\mathbf{M}^{-1}\nabla^2V_d\mathbf{M}^{-1} + (\mathbf{g}_i^T\mathbf{g}_i)^{-1}\mathbf{g}_i^T\mathbf{J}_2\mathbf{M}_d^{-1}\\
&+K_2K_IK_3\mathbf{g}_i^T\mathbf{M}_d^{-1}\Bigg]\mathbf{p}\\
&-\Big(K_vK_2\mathbf{g}_i^T\mathbf{M}_d^{-1}\mathbf{g}_i + K_3\Big)K_I\zeta,
\end{aligned} \tag{6.37}$$

and

$$\begin{aligned}
\dot{\zeta} = &\Big(K_2\mathbf{g}_i^T\mathbf{M}^{-1} + K_3K_1\mathbf{g}_i^T\mathbf{M}_d^{-1}\mathbf{g}_i\mathbf{g}_i^T\mathbf{M}^{-1}\Big)\nabla V_d\\
&+K_3\mathbf{g}_i^T\mathbf{M}_d^{-1}\mathbf{p}.
\end{aligned} \tag{6.38}$$

The controller, composed by the control law (6.37) and the integrator (6.38), does not require the information of the constant disturbance δ_d, as desired. By construction, the dynamics (6.30) in a closed loop with the integral action controller (6.37)-(6.38) can be written in the form (6.31). The Hamiltonian form of the full closed-loop dynamics ensures the stability of the desired equilibrium. Indeed, the Hamiltonian in (6.32) has a minimum at the desired equilibrium $\mathbf{z}^\star$ and it qualifies as a Lyapunov function for the dynamics (6.31). The time derivative of H_z is

$$\begin{aligned}\dot{H}_z &= -K_1 \nabla^T V_d(\mathbf{z}_1)\mathbf{M}^{-1}\mathbf{g}_i\mathbf{g}_i^T\mathbf{M}^{-1}\nabla V_z - K_v \mathbf{z}_2^T \mathbf{M}_d^{-1}\mathbf{g}_i\mathbf{g}_i^T\mathbf{M}_d^{-1}\mathbf{z}_2 \\ &\quad -K_I\Gamma_3 K_I (z_3 - z_3^\star)^2 \\ &\leq 0,\end{aligned}$$

which ensures stability. Asymptotic stability follows using LaSalle arguments and verifying that the maximum invariant set included in $\mathcal{S} = \{(\mathbf{z}_1, \mathbf{z}_2, z_3) | \mathbf{g}_i^T\mathbf{M}^{-1}\nabla V_z = 0, \mathbf{g}_i^T\mathbf{M}_d^{-1}\mathbf{z}_2 = 0, z_3 = z_3^\star\}$ is the desired equilibrium $\mathbf{z}^\star$.

6.4.2 Control design for nonprehensile systems

In this section, the IDA-PBC method is used to design controllers for the DoD, the BnB, and the eccentric DoD. These examples show how a passivity-based framework can be used to solve the control problem of nonprehensile planar rolling manipulation.

6.4.3 Case studies

6.4.3.1 Disk on disk

Dynamic Model. The DoD is a rolling-balancing system shown in Fig.6.2. The dynamics of the DoD can be described as displayed in Section 6.3.2.1. However, now we derive the dynamics in the pH form. Besides, we write the dynamics in terms of the angle of the hand θ_h and the deviation angle of object respect to the upright position $\varphi = \theta_h + \dfrac{s_h}{\rho_h}$. By overwriting the configuration vector $\mathbf{q}$ as $\mathbf{q} = \begin{bmatrix}\theta_h & \varphi\end{bmatrix}^T$, the DoD model takes the following pH form

$$\begin{bmatrix}\dot{\mathbf{q}} \\ \dot{\mathbf{p}}\end{bmatrix} = \begin{bmatrix}\mathbf{O}_2 & \mathbf{I}_2 \\ -\mathbf{I}_2 & \mathbf{O}_2\end{bmatrix}\begin{bmatrix}\nabla_q H \\ \nabla_p H\end{bmatrix} + \begin{bmatrix}\mathbf{0_2} \\ \mathbf{g}_i\end{bmatrix} u, \tag{6.39}$$

where $\mathbf{g}_i = \begin{bmatrix}1 & 0\end{bmatrix}^T$. The Hamiltonian function is

$$H(\mathbf{q},\mathbf{p}) = \frac{1}{2}\mathbf{p}^T M^{-1}\mathbf{p} + V(\mathbf{q}). \tag{6.40}$$

The elements of the mass matrix $\mathbf{M}(\mathbf{q})$ differ from those in Section 6.3.2.1 because of the new definition of $\mathbf{q}$. Therefore, the elements of $\mathbf{M}(\mathbf{q})$ are given by $m_{11} = \rho_h^2 m_o + I_h$, $m_{12} = -m_o\rho_h(\rho_o + \rho_h)$ and $m_{22} = 2m_o(\rho_o + \rho_h)^2$. The expression of the potential energy is instead $V(q) = V_0\cos(\varphi)$, with $V_0 = m_o g(\rho_o + \rho_h)$.

IDA-PBC Controller. The objective is to design a IDA-PBC controller for the DoD system that stabilises the point $q^* = (\theta_h^*,\ 0)$, where θ_h^* is the desired equilibrium for angle of the hand. This problem is solved by using energy shaping and damping injection as described in Section 6.4.1.2. That is, the control design aims to find a function V_d and matrices $\mathbf{M}_d$ and $\mathbf{J}_2$ that solve the KE-ME and PE-ME, (6.24) and (6.25) respectively. Thus, the energy shaping control is obtained from (6.26) and the damping injection control from (6.27).

Since the mass matrix $\mathbf{M}(\mathbf{q})$ of the DoD is constant, i.e., it does not depend on the coordinates $\mathbf{q}$, the desired mass matrix $\mathbf{M}_d$ is selected as a constant matrix as follows

$$\mathbf{M}_d = \begin{bmatrix} a_{11} & a_{12} \\ a_{12} & a_{22} \end{bmatrix}$$

where a_{11}, a_{12} and a_{22} are free constant parameters. To simplify the notation, we note

$$\mathbf{M}_d\mathbf{M}^{-1} = -\begin{bmatrix} \gamma & \delta \\ \alpha & \beta \end{bmatrix}.$$

Then, the PE-ME (6.25) is as follows

$$\begin{aligned} \begin{bmatrix} 0 & 1 \end{bmatrix} \left\{ \begin{bmatrix} 0 \\ -V_0\sin(\varphi) \end{bmatrix} + \begin{bmatrix} \gamma & \delta \\ \alpha & \beta \end{bmatrix} \begin{bmatrix} \nabla_{\theta_h} V_d \\ \nabla_{\varphi} V_d \end{bmatrix} \right\} &= 0 \\ -V_0\sin(\varphi) + \alpha\ \nabla_{\theta_h} V_d + \beta\ \nabla_{\varphi} V_d &= 0. \end{aligned} \tag{6.41}$$

A solution of the partial differential equation (6.41) for V_d, obtained by using a symbolic software (e.g. Mathematica, Maple), is

$$V_d(q) = -\frac{1}{\beta}V_0\cos(\varphi) + \frac{k_2}{2}\left(\theta_h - \frac{\alpha}{\beta}\varphi - k_1\right)^2 \tag{6.42}$$

where $k_1, k_2 \in \mathbb{R}$ are free constant parameters to be selected such that the potential function has a minimum at the desired equilibrium.

Since $\mathbf{M}_d$ was chosen as a constant matrix, it is clear that the KE-ME (6.24) is satisfied by selecting $\mathbf{J}_2(\mathbf{q},\mathbf{p}) = \mathbf{O}_2$. The energy shaping design also requires that $\mathbf{M}_d$ is positive definite and that V_d has an isolated minimum at the desired equilibrium $\mathbf{q}^\star$.

The minimum of V_d is assigned by ensuring that the Jaccobian zero when it is evaluated at $\mathbf{q}^\star$ and Hessian is positive when it is evaluated at $\mathbf{q}^\star$. These conditions are verified through

R-I) $\nabla_q V_d(q)|_{q=q^*} = 0 \Leftrightarrow \left[\begin{array}{c} k_2 \left(\theta_h - \frac{\alpha}{\beta}\varphi - k_1 \right) \\ \frac{V_0}{\beta}\sin(\varphi) - \frac{k_2\alpha}{\beta}\left(\theta_h - \frac{\alpha}{\beta}\varphi - k_1 \right) \end{array} \right] \Bigg|_{q=q^*} = 0$

which is satisfied if $k_1 = \theta_h^*$.

R-II) $\nabla_q^2 V_d(q)|_{q=q^*} > 0 \Leftrightarrow \left[\begin{array}{cc} k_2 & -k_2\frac{\alpha}{\beta} \\ -k_2\frac{\alpha}{\beta} & \frac{V_0}{\beta}\cos(\varphi) + k_2\left(\frac{\alpha}{\beta}\right)^2 \end{array} \right] \Bigg|_{q=q^*} > 0$

which is satisfied provided that $k_2 > 0$ and $\beta > 0$ (equivalently $a_{12}m_{12} - a_{22}m_{11} > 0$).

The positive definiteness of M_d is ensured if $a_{11} > 0$ and $a_{11}a_{22} - a_{12}^2 > 0$.

Figure 6.4 shows that effectively the potential energy has a minimum at the desired equilibrium $(\theta_h^\star, \varphi^\star) = (0, 0)$ (the parameter values used to create the figure satisfy all the requirements R-I and R-II above).

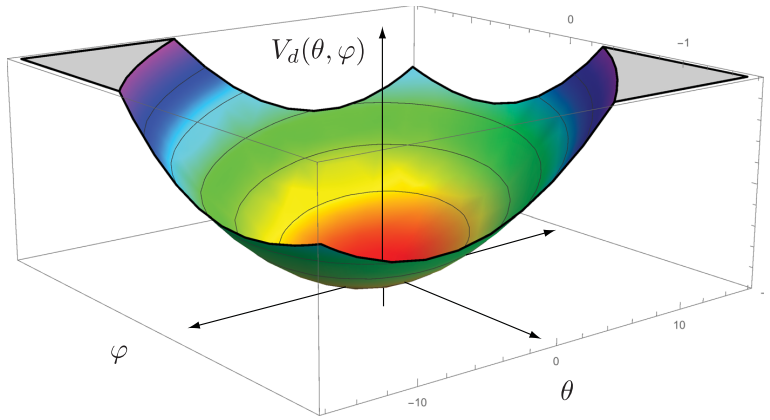

Fig. 6.4: Desired potential energy for the DoD case study with the pH formalism. In this picture $\theta_h = \theta$.

Finally, the control law is computed from (6.26) and (6.27) as follows

$$u = u_{es} + u_{di} = \\ -\frac{\delta}{\beta}\nabla_\varphi V + k_2\left(\frac{\gamma\beta - \delta\alpha}{\beta}\right)\left(\theta_h - \frac{\alpha}{\beta}\varphi - \theta_h^\star\right) + K_v\,\beta\,\sigma\left(\dot{\theta}_h - \frac{\alpha}{\beta}\dot{\varphi}\right) \quad (6.43)$$

where $\sigma = \dfrac{m_{11}m_{22} - m_{12}^2}{a_{11}a_{22} - a_{12}^2}$ and the free parameters a_{11}, a_{12}, a_{22}, k_2 and K_v should satisfy

$$\begin{aligned} &a_{11} > 0, \quad k_2 > 0, \quad K_v > 0, \\ &a_{11}a_{22} - a_{12}^2 > 0, \\ &a_{12}m_{12} - a_{22}m_{11} > 0. \end{aligned}$$

Thus, the dynamics of the DoD system (6.39) in closed loop with the controller (6.43) can be written in the pH form

$$\begin{bmatrix} \dot{\mathbf{q}} \\ \dot{\mathbf{p}} \end{bmatrix} = \begin{bmatrix} \mathbf{O}_2 & \mathbf{M}^{-1}\mathbf{M}_d \\ -\mathbf{M}_d\mathbf{M}^{-1} & -K_v\mathbf{g}_i\mathbf{g}_i^T \end{bmatrix} \begin{bmatrix} \nabla_q H_d \\ \nabla_p H_d \end{bmatrix} \tag{6.44}$$

with

$$H_d = \frac{1}{2}\mathbf{p}^T\mathbf{M}_d^{-1}\mathbf{p} + V_d(\mathbf{q}).$$

Asymptotic stability of the desired equilibrium follows directly from the fact that the closed-loop dynamics has a pH form and the fact that the output $y_d = K_v\mathbf{g}_i^T\mathbf{M}_d^{-1}\mathbf{p}$ is dectable [323].

Integral Controller. In this section, the dynamics (6.44) of the DoD in closed loop with the IDA-PBC controller subject to disturbances is considered. Under this scenario, the dynamics is described as

$$\begin{bmatrix} \dot{\mathbf{q}} \\ \dot{\mathbf{p}} \end{bmatrix} = \begin{bmatrix} \mathbf{O}_2 & \mathbf{M}^{-1}\mathbf{M}_d \\ -\mathbf{M}_d\mathbf{M}^{-1} & -K_v\mathbf{g}_i\mathbf{g}_i^T \end{bmatrix} \begin{bmatrix} \nabla_q H_d \\ \nabla_p H_d \end{bmatrix} + \begin{bmatrix} \mathbf{0_2} \\ \mathbf{g}_i \end{bmatrix} (v + \delta_d), \tag{6.45}$$

where v is the input used for integral control and δ_d is the disturbance. As shown in Section 6.4.1.3 the control law (6.37)-(6.38), specialised for the DoD case, compensates for the action of the disturbance and it preserves the stability of the desired equilibrium $\mathbf{q}^\star$. The IDA-PBC controller and the integral action controller were tested in both simulation and experimental setup. The results can be found in [82]. The results showed satisfactory performance of the closed loop and smooth time history of the control inputs and variables of the system.

6.4.3.2 Ball and beam

Dynamic Model. The BnB system shown in Fig. 6.3 is another rolling-balancing benchmark addressed to test the controller addressed in this section. Now, we come back to the original definition of the configuration vector $\mathbf{q}$ as in Section 6.3.2.2, that is $\mathbf{q} = \begin{bmatrix} \theta_h & s_h \end{bmatrix}^T$. In these coordinates, the BnB model takes the pH form (6.39) with $\mathbf{g}_i = \begin{bmatrix} 1 & 0 \end{bmatrix}^T$, the potential function given by

$$V(\mathbf{q}) = m_o g[(d_h + \rho_o)\cos(\theta_h) - s_h \sin(\theta_h)], \tag{6.46}$$

and the mass matrix elements as in Section 6.3.2.2.

IDA-PBC Controller. The control objective for the BnB system is to stabilize the equilibrium $\mathbf{q}^\star = (0, s_h^\star)$, where $s_h^\star \in \mathbb{R}$ is the desired position of the ball on the beam. The control design follows the procedure proposed in [277] to compute energy shaping controllers for planar rolling manipulations, that is for systems in the form (6.19).

The procedure in [277] can be summarised as follows. Consider the vector of coordinates $\mathbf{q} = \begin{bmatrix} q_1 & q_2 \end{bmatrix}^T$ and the desired mass matrix parametrized as follows

$$\mathbf{M}_d(\mathbf{q}) = \Delta \begin{bmatrix} a_{11}(\mathbf{q}) & a_{12}(\mathbf{q}) \\ a_{12}(\mathbf{q}) & a_{22}(\mathbf{q}) \end{bmatrix}, \tag{6.47}$$

where $\Delta = m_{11}(\mathbf{q})m_{22}(\mathbf{q}) - m_{12}^2(\mathbf{q}) > 0$, which allows to write the PE-ME (6.25) as

$$\mathbf{e}_2^T \left(\nabla_q V(\mathbf{q}) - \mathbf{\Gamma}(\mathbf{q})\nabla_q V_d(\mathbf{q})\right) = 0, \tag{6.48}$$

with

$$\mathbf{\Gamma}(\mathbf{q}) = \begin{bmatrix} a_{11}m_{22} - a_{12}m_{12} & a_{12}m_{11} - a_{11}m_{12} \\ a_{12}m_{22} - a_{22}m_{12} & a_{22}m_{11} - a_{12}m_{12} \end{bmatrix}. \tag{6.49}$$

The PDE (6.48) can be equivalently written as

$$\nabla_{q_2} V(\mathbf{q}) + \alpha(\mathbf{q})\nabla_{q_1} V_d(\mathbf{q}) + \beta(\mathbf{q})\nabla_{q_2} V_d(\mathbf{q}) = 0. \tag{6.50}$$

with

$$\alpha(\mathbf{q}) = a_{22}(\mathbf{q},)m_{12}(\mathbf{q}) - a_{12}(\mathbf{q})m_{22}(\mathbf{q}), \tag{6.51}$$

$$\beta(\mathbf{q}) = a_{12}(\mathbf{q},)m_{12}(\mathbf{q}) - a_{22}(\mathbf{q})m_{11}(\mathbf{q}). \tag{6.52}$$

Then, the scalar functions $\alpha(\mathbf{q}, \mathbf{c}_1)$ and $\beta(\mathbf{q}, \mathbf{c}_1)$ can be chosen to obtain a suitable solution of (6.50) such that $V_d(\mathbf{q})$ satisfies **C.2**. Once $\alpha(\mathbf{q})$ and $\beta(\mathbf{q})$ are selected, the entries $a_{12}(\mathbf{q})$ and $a_{22}(\mathbf{q})$ of the desired mass matrix are computed as

$$a_{12}(\mathbf{q}) = -\frac{\alpha(\mathbf{q})m_{11}(\mathbf{q}) + \beta(\mathbf{q})m_{12}(\mathbf{q})}{\Delta}, \tag{6.53}$$

$$a_{22}(\mathbf{q}) = -\frac{\alpha(\mathbf{q})m_{12}(\mathbf{q}) + \beta(\mathbf{q})m_{22}(\mathbf{q})}{\Delta}. \tag{6.54}$$

By this construction, the desired mass matrix is symmetric, and thus the condition **C.1** is fulfilled if and only if $a_{11}(\mathbf{q}) > 0$ and $a_{11}(\mathbf{q})a_{22}(\mathbf{q}) - a_{12}^2(\mathbf{q}) > 0$. Therefore, by selecting a_{11} as

$$a_{11}(\mathbf{q}) = \frac{k_a a_{12}^2(\mathbf{q})}{a_{22}(\mathbf{q}, \mathbf{c}_1)} > 0, \tag{6.55}$$

where $k_a > 1$ is a constant, the positiveness of $\mathbf{M}_d$ is satisfied if

$$\alpha(\mathbf{q})m_{12}(\mathbf{q}) + \beta(\mathbf{q})m_{22}(\mathbf{q}) < 0. \tag{6.56}$$

If this condition cannot be satisfied, then it is necessary to re-design $\alpha(\mathbf{q})$ and $\boldsymbol{\beta}(\mathbf{q})$ and find another solution for (6.50). Finally, the desired mass matrix takes the form

$$\mathbf{M}_d(\mathbf{q}) = \begin{bmatrix} -\dfrac{k_a(\alpha m_{11} + \beta m_{12})^2}{(\alpha m_{12} + \beta m_{22})} & -(\alpha m_{11} + \beta m_{12}) \\ -(\alpha m_{11} + \beta m_{12}) & -(\alpha m_{12} + \beta m_{22}) \end{bmatrix}. \tag{6.57}$$

In addition, the degree of freedom given by the matrix $\mathbf{J}_2(\mathbf{q}, \mathbf{p})$ is used to satisfy the KE-ME (6.24). The interconnection matrix $\mathbf{J}_2$ has the following structure

$$\mathbf{J}_2(\mathbf{q}, \mathbf{p}) = \begin{bmatrix} 0 & j_2(\mathbf{q}, \mathbf{p}) \\ -j_2(\mathbf{q}, \mathbf{p}) & 0 \end{bmatrix}, \tag{6.58}$$

with $j_2(\mathbf{q}, \mathbf{p})$ a scalar function. Since $\mathbf{e}_2^T \mathbf{J}_2(\mathbf{q}, \mathbf{p}) = -j_2(\mathbf{q}, \mathbf{p})\mathbf{e}_1^T$, then the KE-ME (6.24) can be expressed as

$$\begin{aligned} &\mathbf{e}_2^T \nabla_q(\mathbf{p}^T \mathbf{M}^{-1}(\mathbf{q})\mathbf{p}) - \mathbf{e}_2^T \mathbf{M}_d(\mathbf{q})\mathbf{M}^{-1}(\mathbf{q})\nabla_q(\mathbf{p}^T \mathbf{M}_d^{-1}(\mathbf{q})\mathbf{p}) \\ &\quad - 2j_2(\mathbf{q}, \mathbf{p})\mathbf{e}_1^T \mathbf{M}_d^{-1}(\mathbf{q})\mathbf{p} = 0. \end{aligned} \tag{6.59}$$

The scalar function $j_2(\mathbf{q}, \mathbf{p})$ can be from (6.59) as follows

$$\begin{aligned} j_2(\mathbf{q}, \mathbf{p}) = \left(2\mathbf{e}_1^T \mathbf{M}_d^{-1}(\mathbf{q})\mathbf{p}\right)^{-1} \big(&\mathbf{e}_2^T \nabla_q(\mathbf{p}^T \mathbf{M}^{-1}(\mathbf{q})\mathbf{p}) \\ &- \mathbf{e}_2^T \mathbf{M}_d(\mathbf{q})\mathbf{M}^{-1}(\mathbf{q})\nabla_q(\mathbf{p}^T \mathbf{M}_d^{-1}(\mathbf{q})\mathbf{p})\big), \end{aligned} \tag{6.60}$$

and the IDA-PBC law can be finally computed from (6.26).

Notice that the method used to satisfy the KE-ME, inspired by [264], provides a solution that is not always well-defined. Close to the equilibrium, the numerator of (6.60), which has a quadratic dependence on $\mathbf{p}$, tends towards zero faster than the denominator, which depends linearly on $\mathbf{p}$, which would avoid singularities. Despite this, a study about the denominator of the relation (6.60) reveals that, far from the equilibrium, it might be nullified if the equality $(\alpha(\mathbf{q})m_{12}(\mathbf{q}) + \beta(\mathbf{q})m_{22}(\mathbf{q}))p_1 = (\alpha(\mathbf{q})m_{11}(\mathbf{q}) + \beta(\mathbf{q})m_{12}(\mathbf{q}))p_2$ holds. This situation is addressed in practice by saturating the denominator of (6.60) when its absolute value is smaller than a suitable threshold. The simplification of the design proposed here is at the expense of the presence of possible singular solutions of (6.60), but these can always be numerically managed in the controller implementation. Recently, this problem has been overcome in [8].

For the BnB case study, the functions $\alpha(\mathbf{q})$ and $\beta(\mathbf{q})$ are selected as $\alpha(\theta_h) = k\text{sinc}(\theta_h)$ and $\beta(\theta_h) = -\text{sinc}(\theta_h)$, where $k \in \mathbb{R}$ is a constant parameter. Notice that the $\text{sinc}(\cdot)$ function is analytic everywhere. Assuming

the domain of interest as $-\pi < \theta_h < \pi$, then $0 < \text{sinc}(\theta_h) < 1$. Using these functions in (6.50), the PE-ME becomes

$$-m_o g \sin(\theta_h) + k\text{sinc}(\theta_h)\nabla_{\theta_h} V_d(\mathbf{q}) - \text{sinc}(\theta_h)\nabla_{s_h} V_d(\mathbf{q}) = 0. \quad (6.61)$$

A solution of (6.61) is given by

$$V_d(\mathbf{q}) = \frac{m_o g \theta_h^2}{2k} + f\left(\frac{\theta_h + k s_h}{k}\right), \quad (6.62)$$

where $f(\cdot)$ is a function to be selected to satisfy **C.2**. Then, $f(\cdot)$ is chosen such that the desired potential function (6.62) results as follows

$$V_d(\mathbf{q}) = \frac{m_o g \theta_h^2}{2k} - \cos\left(\frac{k_f}{k}\left[\theta_h + k\left(s_h - s_h^\star\right)\right]\right), \quad (6.63)$$

with $k_f \in \mathbb{R}$ a constant parameter. The Jacobian of $V_d(\mathbf{q})$ is computed to verify that $\mathbf{q}^\star$ is a minimum of the desired potential function (6.63), which yields

$$\nabla V_d(\mathbf{q}) = \begin{bmatrix} \dfrac{m_o g}{k}\theta_h + \dfrac{k_f}{k}\sin\left(\dfrac{k_f}{k}[\theta_h + k(s_h - s_h^\star)]\right) \\ k_f \sin\left(\dfrac{k_f}{k}[\theta_h + k(s_h - s_h^\star)]\right) \end{bmatrix}, \quad (6.64)$$

where it is possible to verify that $\nabla V_d(\mathbf{q})$ is zero at $\mathbf{q}^\star$. Then, the corresponding Hessian is given by

$$\nabla^2 V_d(\mathbf{q}) = \begin{bmatrix} \dfrac{m_o g}{k} + \dfrac{k_f^2}{k^2}\cos\phi & \dfrac{k_f^2}{k}\cos\phi \\ \dfrac{k_f^2}{k}\cos\phi & k_f^2\cos\phi \end{bmatrix}, \quad (6.65)$$

with $\phi = \dfrac{k_f}{k}\left[\theta_h + k\left(s_h - s_h^\star\right)\right]$. It is possible to verify that $\nabla^2 V_d(\mathbf{q})$ is positive definite at the desired equilibrium $\mathbf{q}^\star$ if $k > 0$ and $k_f \neq 0$. The conditions on the Jacobian and the Hessian of $V_d(\mathbf{q})$ ensure that the desired potential function $V_d(\mathbf{q})$ has a minimum at the desired equilibrium $\mathbf{q}^\star$.

In addition, the inequality (6.56) must be satisfied to ensure the positiveness of $\mathbf{M}_d$. Using the selected functions $\alpha(\mathbf{q})$ and $\boldsymbol{\beta}(\mathbf{q})$, the inequality (6.56) becomes

$$k m_{12} - m_{22} < 0, \quad (6.66)$$

which has the straightforward solution $k < \dfrac{m_{22}}{m_{12}}$. Since $\dfrac{m_{22}}{m_{12}} > 0$, the parameter k has to be selected to satisfy $0 < k < \dfrac{m_{22}}{m_{12}}$.

Finally, the entries $a_{12}(\mathbf{q})$ and $a_{22}(\mathbf{q})$ of $\mathbf{M}_d(\mathbf{q})$ are computed from (6.53) and (6.54) as follows

$$a_{12}(\mathbf{q}) = -\frac{\text{sinc}(\theta_h)(km_{11}(s_h) - m_{12})}{\Delta}, \qquad (6.67)$$
$$a_{22}(\mathbf{q}) = -\frac{\text{sinc}(\theta_h)(km_{12} - m_{22})}{\Delta},$$

while $a_{11}(\mathbf{q})$ is computed as in (6.55). Therefore, the desired mass matrix is

$$\mathbf{M}_d(\mathbf{q}) = \begin{bmatrix} -\dfrac{k_a\left(km_{11}(s_h) - m_{12}\right)^2}{(km_{12} - m_{22})} & -\text{sinc}(\theta_h)\left(km_{11}(s_h) - m_{12}\right) \\ -\text{sinc}(\theta_h)\left(km_{11}(s_h) - m_{12}\right) & -\text{sinc}(\theta_h)(km_{12} - m_{22}) \end{bmatrix}. \qquad (6.68)$$

The KE-ME (6.24) is satisfied using (6.60), and the IDA-PBC control law is computed from (6.28).

Figures 6.5 and 6.6 show the desired potential function (6.63) and a trajectory from a particular initial condition. As expected, the trajectory converges to the minimum, that is the desired equilibrium $\mathbf{q}^\star$. An exhaustive simulation study of the the closed loop has been presented in [277].

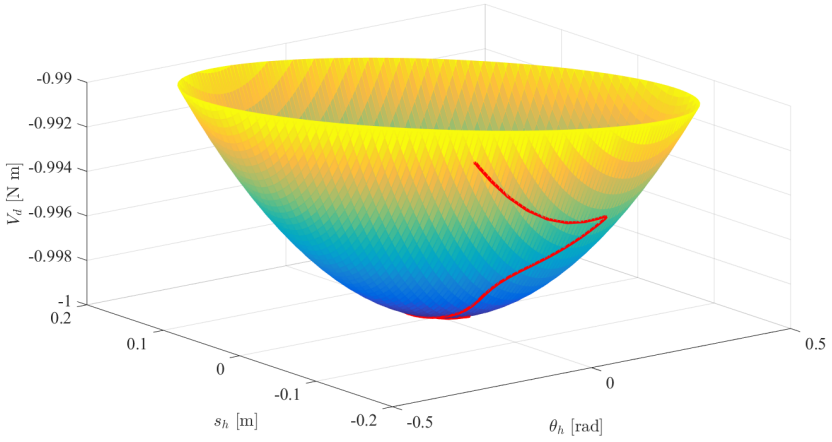

Fig. 6.5: Desired potential function and coordinate trajectory for the BnB case study with the pH formalism.

6.4.3.3 Eccentric disk-on-disk

Dynamic Model. The eccentric DoD system is represented in Fig. 6.7 [277]. In this system, the hand is the actuated bottom disk and the object is the

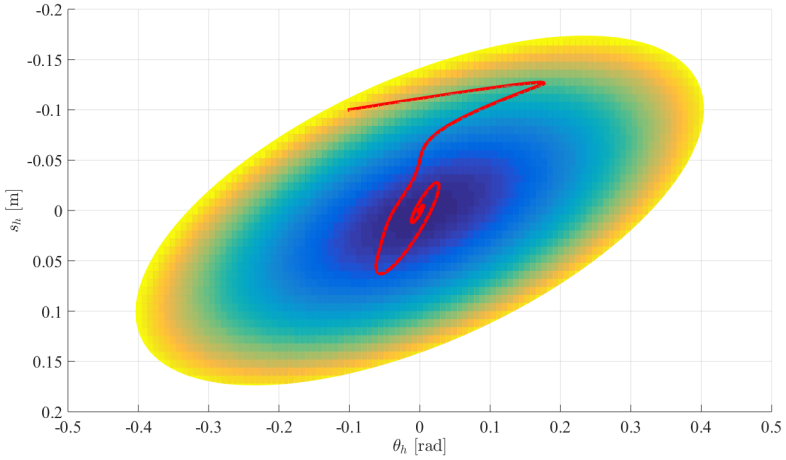

Fig. 6.6: Desired potential function and coordinate trajectory for the BnB case study with the pH formalism.

non-actuated disk that sits on top. With respect to the classic DoD seen before, the hand's CoM and the actuation point are at a distance $\lambda > 0$. It can be shown that the mass matrix elements are $m_{11} = c_{b1} + c_{b2}\cos\left(\frac{s_h}{\rho_h}\right)$, $m_{12} = c_{b3} + c_{b4}\cos\left(\frac{s_h}{\rho_h}\right)$, and $m_{22} = I_o\kappa_r^2 + m_o\rho_o^2\kappa_r^2$, where $c_{b1} = I_h + I_o + \lambda^2(m_h + m_o) + m_o(\rho_h + \rho_o)^2$, $c_{b2} = 2\lambda m_o(\rho_h + \rho_o)$, $c_{b3} = I_o\kappa_r + m_o\frac{(\rho_h+\rho_o)^2}{\rho_h}$, and $c_{b4} = m_o\lambda\rho_o\kappa_r$. The potential energy (6.4) for the eccentric DoD is

$$V(\mathbf{q}) = g(m_o(\rho_h + \rho_o)\cos\left(\theta_h + \frac{s_h}{\rho_h}\right) + (m_o + m_h)\lambda\cos(\theta_h)). \tag{6.69}$$

A detailed derivation of this model can be found in [277].

IDA-PBC Controller. The control objective is to balance the object on top of the hand. In this configuration, the CoM of the hand can be placed above or below its center of actuation. In both cases it is possible, under a suitable change of coordinates, to express the desired equilibrium point as $\mathbf{q}^\star = (0, 0)$ in both cases.

The controller for the eccentric DoD is computed using the same procedure used for the BnB in Section 6.4.3.2. Thus, the functions $\alpha(\mathbf{q})$ and $\beta(\mathbf{q})$ are selected as $\alpha(\theta_h, s_h) = \text{sinc}\left(\theta_h + \frac{s_h}{\rho_h}\right)$ and $\beta(\theta_h, s_h, k) = k\text{sinc}\left(\theta_h + \frac{s_h}{\rho_h}\right)$, where $k \in \mathbb{R}$ is a constant parameter. The function $\text{sinc}(\cdot)$ satisfies $0 < \text{sinc}\left(\theta_h + \frac{s_h}{\rho_h}\right) < 1$ in the domain of interest $-\pi < \left(\theta_h + \frac{s_h}{\rho_h}\right) < \pi$. Using

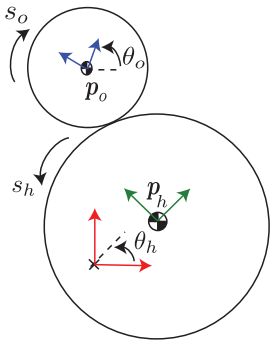

Fig. 6.7: A schematic of the eccentric DoD system.

the selected function $\alpha(\mathbf{q})$ and $\beta(\mathbf{q})$ in (6.50) yields

$$\begin{aligned} -c_v \sin\left(\theta_h + \frac{s_h}{\rho_h}\right) + \operatorname{sinc}\left(\theta_h + \frac{s_h}{\rho_h}\right) \nabla_{\theta_h} V_d(\mathbf{q}) \\ + k\operatorname{sinc}\left(\theta_h + \frac{s_h}{\rho_h}\right) \nabla_{s_h} V_d(\mathbf{q}) = 0, \end{aligned} \tag{6.70}$$

where $c_v = m_o g \dfrac{\rho_h + \rho_o}{\rho_h}$ is a positive constant parameter. A solution for (6.70) is given by

$$V_d(\mathbf{q}) = \frac{c_v \theta_h^2 (\rho_h - k) + 2 c_v \theta_h s_h}{2\rho_h} + f(s_h - k\theta_h), \tag{6.71}$$

where $f(\cdot)$ is a function to be chosen. To satisfy **C**.2, $f(\cdot)$ is selected such that the desired potential function (6.71) becomes

$$V_d(\mathbf{q}) = \frac{c_v \theta_h^2 (\rho_h - k) + 2 c_v \theta_h s_h}{2\rho_h} + k_f (s_h - k\theta_h)^2, \tag{6.72}$$

where $k_f \in \mathbb{R}$ is a controller gain.

To verify that $\mathbf{q}^\star$ is a minimum for (6.72), the Jacobian and the Hessian of the potential function are computed. The Jacobian is

$$\nabla V_d(\mathbf{q}) = \begin{bmatrix} \dfrac{c_v(-k\theta_h + \theta_h \rho_h + s_h)}{\rho_h} + 2kk_f(k\theta_h - s_h) \\ \dfrac{c_v \theta_h}{\rho_h} - 2kk_f\theta_h + 2k_f s_h \end{bmatrix}, \tag{6.73}$$

where it is possible to verify that $\nabla V_d(\mathbf{q})$ is zero at $\mathbf{q}^\star$. Also, the Hessian of $V_d(\mathbf{q})$ is

$$\nabla^2 V_d(\mathbf{q}) = \begin{bmatrix} c_v + 2k^2 k_f - \dfrac{c_v k}{\rho_h} & -2kk_f + \dfrac{c_v}{\rho_h} \\ -2kk_f + \dfrac{c_v}{\rho_h} & 2k_f \end{bmatrix}. \tag{6.74}$$

It is possible to verify that $\nabla^2 V_d(\mathbf{q})$ is positive definite at the desired equilibrium $\mathbf{q}^\star$ if $k > -\rho_h$ and $k_f > \dfrac{c_v}{2\rho_h(k+\rho_h)}$. These conditions on the Jacobian and Hessian of the desired potential function ensure that $V_d(\mathbf{q})$ has a minimum at the desired equilibrium $\mathbf{q}^\star$.

Following the design procedure sketched out in Section 6.4.3.2, the inequality (6.56) must be solved. Using the functions $\alpha(\mathbf{q})$ and $\beta(\mathbf{q})$ selected above, equation (6.56) yields

$$m_{12}(s_h) + km_{22} < 0, \tag{6.75}$$

which has the straightforward solution $k < -\dfrac{m_{12}(s_h)}{m_{22}}$. Since it is possible to verify that $\rho_h > \dfrac{(c_{b3} - c_{b4})}{m_{22}}$ and together with the previous condition $k > -\rho_h$, then the gain k must satisfy $-\rho_h < k < -\dfrac{c_{b3} - c_{b4}}{m_{22}}$.

Finally, the entries of $\mathbf{M}_d(\mathbf{q})$ are computed as in (6.53) and (6.54)

$$\begin{aligned} a_{12}(\mathbf{q}) &= -\frac{\operatorname{sinc}\left(\theta_h + \dfrac{s_h}{\rho_h}\right)(m_{11}(s_h) + km_{12}(s_h))}{\Delta}, \\ a_{22}(\mathbf{q}) &= -\frac{\operatorname{sinc}\left(\theta_h + \dfrac{s_h}{\rho_h}\right)(m_{12}(s_h) + km_{22})}{\Delta}, \end{aligned} \tag{6.76}$$

while $a_{11}(\mathbf{q})$ is taken as in (6.55). The desired mass matrix is thus positive definite and it can be written as

$$\begin{aligned} &\mathbf{M}_d(\mathbf{q}) \\ &= \begin{bmatrix} \Delta a_{11} & -(m_{11} + km_{12})\operatorname{sinc}\left(\theta_h + \dfrac{s_h}{\rho_h}\right) \\ -(m_{11} + km_{12})\operatorname{sinc}\left(\theta_h + \dfrac{s_h}{\rho_h}\right) & -(m_{12} + km_{22}\operatorname{sinc}\left(\theta_h + \dfrac{s_h}{\rho_h}\right)) \end{bmatrix}. \end{aligned} \tag{6.77}$$

The KE-ME (6.24) is satisfied using (6.60), while the IDA-PBC control law is computed from (6.28). The controller has been implemented in an real setup and the experiments show a satisfactory performance of the closed loop. The results can be found in [277].

6.5 Discussion and conclusion

This chapter investigated the control design for nonprehensile planar rolling manipulation using FLin techniques, PBC methods, and pH theory. The dynamic model of nonprehensile holonomic rolling manipulation systems was presented in its general form and then used for control design purposes.

The first class of controllers presented in this chapter was obtained using FLin, thus requiring the cancellation of all system nonlinearities. Upon certain conditions given by the shapes of the hand the object in contact with it, it has been possible to found a diffeomorphism rendering the original system in a normal form (i.e., a chain of integrators). Therefore, any linear technique can be, in principle, employed. In this chapter, the EFL technique was employed on two benchmark systems: the DoD and the BnB.

The second class of controllers developed in this chapter was designed using IDA-PBC methods and pH dynamics. Two different designs were followed within this framework. First, the classical IDA-PBC procedure to stabilise mechanical systems was used to obtain a controller for the DoD. Also, an integral action controller was added in the loop to robustify the control system against disturbances. It was shown that the closed loop dynamics preserve the pH structure and thus its intrinsic passivity properties. This design requires solving a set of PDEs, which results from the so-called matching equation. To simplify solving PDEs, an alternative procedure was used to design the second class of controllers. This procedure was successfully applied to the BnB and the eccentric DoD systems.

The effectiveness of the controllers presented in this chapter was verified by simulations and experiments on real physical set-ups, and the results reported in [83, 82, 173, 277]. These positive results show that the set of methods presented in this chapter is suitable for controlling nonprehensile planar rolling manipulation systems and provides a potential framework for the control design of general dynamic robotic manipulation tasks. Future research will aim at the development of a framework for a general class of dynamic manipulations.